IEEE Access
Multidisciplinary | Rapid Review | Open Access Journal

Received December 24, 2019, accepted January 3, 2020, date of publication January 10, 2020, date of current version February 6, 2020.

Digital Object Identifier 10.1109/ACCESS.2020.2965643

Retrieval of Gas Temperature and Pressure Based on Rayleigh–Brillouin Spectrum

PENG ZHANG[1], JIAQI XU[1], RUIZHE ZHANG[1], QIAN SUN[2], HANG WU[3], YANGRUI XU[1], BO ZHOU[1,4], AND KUN LIANG[1,4]

[1]Department of Electronic Information and Communication, Huazhong University of Science and Technology, Wuhan 430074, China
[2]Beijing Institute of Space Mechanics and Electricity, Beijing 100076, China
[3]Third Department, China Ship Research and Development Academy, Wuhan 430074, China
[4]Science and Technology on Multi-Spectral Information Processing Laboratory, Huazhong University of Science and Technology, Wuhan 430074, China

Corresponding author: Kun Liang (liangkun@hust.edu.cn)

This work was supported in part by the Joint Research Project between China and The Netherlands under Grant 530-5CDP05, and in part by the Guangxi Innovative Development under Grant GuiKe AA 18118038.

ABSTRACT Optical detection methods such as Rayleigh–Brillouin scattering spectrum can be used for physical parameter measurement in solids, liquids, and gas. In this paper, a new method based on spectral characteristics is proposed to realize temperature and pressure retrieval simultaneously in gas. The characteristics of Rayleigh–Brillouin spectrum are firstly utilized to establish the retrieval model by fitting Tenti-S6 line shape with 3Voigt model at different temperatures and pressures, and then deriving the retrieval equations via regression fitting procedure. Through theoretical and measured error analyses, the characteristic retrieval model based on Rayleigh linewidth and the whole linewidth of Rayleigh–Brillouin scattering spectrum is shown to be optimal. Afterward, the retrieval model is verified using the experimental Rayleigh-Brillouin scattering spectra of N_2 and air. The results indicate that, compared with the current method based on the whole linewidth or line shape of spectrum, the proposed method not only produces lower theoretical and retrieval errors but also can simultaneously retrieve the temperature and pressure of gases. The novel retrieval method provides a new idea for obtaining valuable information on gas parameters and promotes the application of Brillouin lidar remote sensing in meteorology and space science.

INDEX TERMS Deconvolution, pressure measurement, Rayleigh–Brillouin spectrum, retrieval model, remote sensing, temperature measurement.

I. INTRODUCTION

Rayleigh–Brillouin (RB) scattering, as a powerful method for investigating the physical and chemical properties, such as temperature, pressure, and shear viscosity, of an optical medium, has been attracting more and more attention [1]–[3]. Light scattering can be described as the dielectric fluctuation that includes the pressure fluctuations at constant entropy and the entropy fluctuations at constant pressure, and the properties of the medium can be reflected by the RB scattering spectrum [4], [5]. Therefore, the study of RB scattering is helpful both for understanding the properties of the medium and for real applications in the fields of environmental monitoring, defense industry, and space science [6]–[9].

The associate editor coordinating the review of this manuscript and approving it for publication was Md. Moinul Hossain.

Laser detection based on RB scattering has proved to be an effective way of measuring the parameters of optical fiber and seawater, for which the basic principle is establishing the relationships between the properties of the medium (e.g., strain of the fiber, sound speed, salinity, and bulk viscosity) and the characteristic parameters of RB scattering spectrum (e.g., Brillouin shift, Brillouin linewidth). Based on these relationships, the parameters of the medium can then be retrieved from the RB scattering spectrum. In 2014, Wang *et al.* [10] proposed a method of simultaneously measuring the temperature and strain in a local and distributed optical fiber sensor system, in which the strain and temperature are calculated using the echo power and Brillouin shift in backward scattering light, according to the photothermal effect of the optical fiber. In a research on seawater, Liang *et al.* [11] studied the relationships among Brillouin shift and Brillouin linewidth, and the temperature and salinity of the sea water,

and then established a retrieval method for measuring the temperature and salinity of seawater simultaneously, which greatly contributes to temperature and salinity remote sensing in seawater.

The Rayleigh and Brillouin scattering spectra in gas are usually overlapped, allowing the global profile of the RB spectrum to be directly obtained instead of the respective spectral characteristics, as in the method described for seawater and optical fibers. Considering this phenomenon, many physical models for describing the RB spectra of gases are created. Currently, the Tenti-S6 model developed by Tenti *et al*. [12] (1974) is generally considered as the most accurate model for describing the RB spectrum of gas. This model is based on the Wang-Chang–Uhlenbeck [13] equation in molecule collision theory and uses macroscopic transmission coefficients, such as shear viscosity, bulk viscosity, thermal conductivity, and internal specific heat capacity, to describe the microscopic effect in gas. Therefore, through a comparison of the global RB scattering spectrum with the Tenti-S6 model line shape, the physical parameters of the gas can be derived for research [14].

For instance, in 2014, Witschas *et al*. [15], [16] retrieved the temperature of a gas, at an accuracy of 2 K, from the RB spectrum using the Tenti-S6 model in laboratory conditions. In the same year, they showed that the temperature measurements are close to the radiosonde measurements at noon through the temperature profiles from 2 to 15.3 km in outdoor experiments. The temperature difference between the retrieval data and the radiosonde measurements reached up to 5 K below the boundary layer and was smaller than 2.5 K above the boundary layer.

The Tenti-S6 model is helpful for researching the properties of a gas RB spectrum and shows a high agreement with the experimental spectrum, but it is a complex and non-analytical model that is unable to provide a simple representation of the RB scattering spectrum. Another efficient way of retrieving the gas temperature is by establishing the relationship between the gas properties and the overall linewidth of the RB spectrum. In 2017, the relationship between the temperature of the gas and the overall linewidth of the RB scattering spectrum was researched by Liang *et al.* [17]. Based on this relationship, the gas temperature can be retrieved, with the errors of temperature retrieval at 2.9 K in N_2, and 2.5 K in air. The retrieval accuracy meets the requirements for practical application [17]–[20]. In this method, the linewidth can be measured directly, and the pressures of the gases are theoretically calculated according to the barometric height formula [21], [22].

For application in real remote sensing, measuring the gas pressure is also necessary even though this pressure can be obtained from the barometric height formula. According to the relationship of the pressure and RB spectral characteristic parameters, the pressure can be retrieved simultaneously with the temperature retrieval method via dual-parameter models, which are expressed as the function set, and each function is composed of two arbitrary characteristics. Therefore, it is not necessary to determine the pressure from the barometric height formula. The key of this concept is the spectral inner components division, which is used to obtain all characteristic parameters from the whole profile of the RB scattering spectrum and express the pressure and temperature of the gas using these characteristic parameters.

To obtain the inner components of the gas RB scattering spectrum, two analytical models, the 3Gaussian (G3) and 3Voigt (V3) models, were proposed by Witschas [23] and Ma *et al.* [24], respectively. According to the G3 model, the RB scattering line shape can be expressed using three Gaussian functions, one of which represents the Rayleigh scattering peak and two of which represent two Brillouin scattering peaks. On the other hand, the V3 model uses three Voigt functions to express these three peaks and exhibits a better fitting performance than that of the G3 model. Based on these analytical models, the inner Rayleigh peak and Brillouin peaks can be described, and the corresponding characteristic parameters, such as the Brillouin shift, Brillouin linewidth, and Rayleigh linewidth, can be easily obtained. The theoretical research shows that these characteristic parameters of the RB scattering spectrum are all related to the temperature and pressure of the gas [25], [26]. However, the properties of these characteristics and the retrieval model based on them have not been researched.

To retrieve the temperature and pressure of gas simultaneously, we firstly obtain the characteristic parameters of the RB spectrum (e.g., Brillouin shift, Brillouin linewidth, Rayleigh linewidth, and the whole RB linewidth) by comparing the Tenti-S6 model with the V3 model for different pressures and temperatures. The dependence of each characteristic on temperature and pressure is then analyzed, and models based on the relationships among the characteristics, temperature, and pressure are established. Afterward, the optimal model is chosen by analyzing the theoretical and measured errors of these models. Finally, the correctness of the optimal model is analyzed using the experimental data.

The new retrieval method can effectively eliminate the error introduced from the pressure formula and obtain the temperature and pressure of the gas simultaneously, thus providing a novel idea for studying the distribution of temperature and pressure resulting from the air flowing and exchanging in the atmosphere. To some extent, this work is of great significance to meteorology and space science research.

II. PRINCIPLES AND RESEARCH METHOD

A. GENERAL THEORY AND RETRIEVAL MODEL

RB scattering is produced by the density fluctuations of molecular gas. The RB scattering spectrum contains two parts: a central Rayleigh peak, and two Stokes- and anti-Stokes-shifted Brillouin peaks. When the frequency shift of the two Brillouin peaks is smaller than the linewidth of the Rayleigh peak, the three peaks are overlapped and form a mixed profile, which can reflect in the motion of the gas molecules. Because the molecular motion is related to the

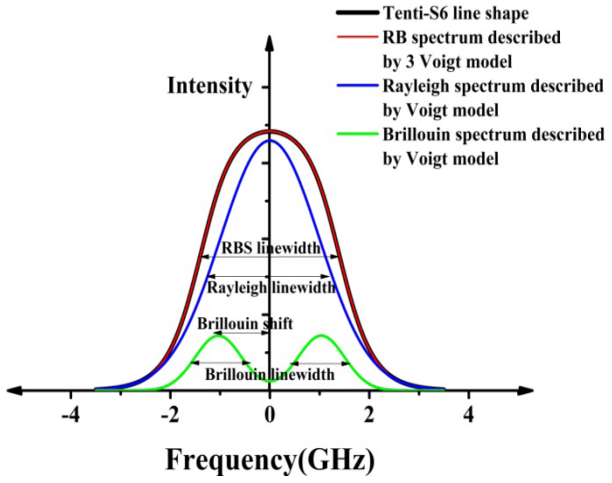

FIGURE 1. Characteristic parameters of Rayleigh–Brillouin spectrum.

temperature and pressure in gas, there will be some relationships between these physical parameters of gas and the characteristics in the RB spectrum, such as Rayleigh linewidth, Brillouin linewidth, Brillouin peaks shift, and linewidth of the whole profile, which can be used for temperature and pressure retrieval in the atmosphere. The relationship between the linewidth of the whole spectrum and the temperature has already been studied [17]. Although the pressure is also related to the linewidth of the whole spectrum, it is not enough to utilize only one characteristic of the spectrum for the simultaneous retrieval of temperature and pressure. Therefore, obtaining the other characteristics is necessary even though these are not easy to determine from the global RB spectrum directly. One way to respectively visualize the spectral parameters is by comparing the simulated RB spectrum generated by the S6 model with the spectra generated by the V3 model, and the fitted characteristics are all shown in Figure 1 as follows.

The V3 model was proposed based on the spectral broadening theory [27], [28], aiming to describe the line shape of RB spectral inner components. In the spectral broadening theory, the line shapes of both Rayleigh and Brillouin scattering will be affected by two kinds of broadening effects: homogeneous broadening and inhomogeneous broadening. The former takes on the Lorentzian line shape, and the latter can be expressed as a Gaussian function. When both effects are considered, the Rayleigh peak or Brillouin peak can be characterized as a Voigt profile V(v), which is expressed as the convolution of a Gaussian function and a Lorentzian function, as shown in Equation (1), according to [24]. The symbol * represents the convolution operation, and v represents the optical frequency.

$$\begin{aligned} V(v) &= L(v;\, \Delta v_L, v_c)^* G(v;\, \Delta v_G, v_c) \\ &= \int_{-\infty}^{+\infty} L(v;\, \Delta v_L, v_c) G(v-\tau;\, \Delta v_G, v_c) d\tau \end{aligned} \quad (1)$$

where G(v; Δv_G, v_c) is the Gaussian function:

$$G\left(v;\, \Delta v_G, v_c\right) = \frac{2\sqrt{\ln 2}}{\sqrt{\pi}\,\Delta v_G} \exp\left[\frac{-4\ln 2\,(v-v_c)^2}{\Delta v_G^2}\right]. \quad (2)$$

L(v; Δv_L, v_c) is the Lorentz function and expressed as

$$L\left(v;\, \Delta v_L, v_c\right) = \frac{2}{\pi}\frac{\Delta v_L}{4\,(v-v_c)^2 + \Delta v_L^2}, \quad (3)$$

where Δv_L and Δv_G are the full widths at half maximum (FWHM) of the Lorentzian and Gaussian profiles, respectively. v_c is the central frequency of the Voigt profile. If we set the intensity of the Rayleigh peak to be I_R, with $v_c = v_0 = 0$, and the intensity of the Brillouin double peaks to be $1-I_R$, with the $v_c = v_b$ or $v_c = v_{-b}$ for the Brillouin frequency shift. The form of the RB scattering profile can be shown as Equation (4).

$$\begin{aligned} 3V(v) = {} & I_R L(v;\, \Delta v_L, v_0)^* G(v;\, \Delta v_G, v_0) \\ & + 0.5(1-I_R) L(v;\, \Delta v_L, v_b) \\ & {}^* G(v;\, \Delta v_G, v_b) \\ & + 0.5(1-I_R) L(v;\, \Delta v_L, v_{-b})^* G(v;\, \Delta v_G, v_{-b}) \end{aligned} \quad (4)$$

To analyze how the variation law of the spectral characteristics varies with the changes in temperature and pressure, the simulation of the RB scattering spectrum produced by the Tenti-S6 model for different temperatures and pressures was compared with V3 to obtain the spectral characteristic parameters in different temperatures and pressures.

The Tenti-S6 model is a well-known theory for describing the spectral line shape of scattered light in monomolecular gas and has been proved to perform well for N_2, O_2, and air gases [5]. To obtain the temperature and pressure retrieval model, the temperature T should be regarded as a dependent variable, while two characteristic parameters X and Y of the spectrum (such as Brillouin shift, Brillouin linewidth, Rayleigh linewidth, or RB spectral linewidth) should be independent variables, and a least-square fitting is used to determine a function $f_1(X, Y)$. The pressure retrieval model $f_2(X, Y)$ of gas can be treated the same way. The dual-parameter retrieval model can then be described as Equation (5):

$$\begin{cases} T = f_1(X, Y) \\ P = f_2(X, Y), \end{cases} \quad (5)$$

where X and Y represent the two kinds of characteristics of the spectrum, respectively.

According to meteorology, in the northern hemisphere and in the lower atmosphere (0 to 15 km of the vertical height) [29], the typical range of atmospheric temperature is about 210–350 K, and that of the pressure is about 0.1–1.5 bar. With this information taken into account, the spectra of N_2 are firstly simulated using the Tenti-S6 model with temperature from 210 K to 350 K and pressure from 0.1 bar to 1.5 bar, because N_2 is the main component of the real atmosphere, and its property is close to that of ideal gas. In the simulation section, the four kinds of spectral

characteristics of each condition are obtained by comparing the RB spectral profile produced by the S6 model with that produced by the V3 model. We can then obtain 225 sets of characteristic parameters in different temperatures and pressures. The Brillouin shift of N_2 is displayed in Table 1 as an example.

Selecting two of the four spectral characteristics at a time, we can get six groups of characteristics that vary as the temperature and pressure changes. These groups are denoted by A (Brillouin shift, Brillouin linewidth), B (Brillouin shift, Rayleigh linewidth), C (Brillouin shift, RBS linewidth), D (Brillouin linewidth, Rayleigh linewidth), E (Brillouin linewidth, RBS linewidth), and F(Rayleigh linewidth, RBS linewidth). Using the least-square fitting method, the analytical formulas of six sets of retrieval models can be obtained according to the method depicted by Equation (5).

For instance, if we choose Group A, the temperature T and pressure P can be expressed as functions of Brillouin shift V_b and Brillouin linewidth Γ_b of the spectrum, as follows:

$$\begin{aligned} T =\ & 1294.46 - 1767.28V_b - 1982.96\Gamma_b + 839.53V_b^2 \\ & + 1036.21\Gamma_b^2 + 2010.60V_b\Gamma_b \\ & - 155.815V_b^3 - 75.61\Gamma_b^3 - 761.40V_b\Gamma_b^2 \\ & - 173.67V_b^2\Gamma_b \end{aligned} \tag{6}$$

$$\begin{aligned} P =\ & -6.23 + 14.91V_b + 8.56/\Gamma_b - 8.79V_b^2 \\ & + 0.68/\Gamma_b^2 - 22.28V_b/\Gamma_b \\ & + 0.854V_b^3 - 0.902/\Gamma_b^3 + 2.31V_b/\Gamma_b^2 \\ & + 11.65V_b^2/\Gamma_b \end{aligned} \tag{7}$$

All the rest of the groups can be determined in the same way.

B. THEORETICAL ANALYSIS OF RETRIEVAL MODEL FOR TEMPERATURE AND PRESSURE

How the properties of the characteristics depend on the temperature or pressure will affect the accuracy of temperature and pressure retrieval. The concept of retrieval theoretical error, namely the temperature or pressure retrieval error caused by a 1 MHz measurement error in the characteristics, is used to quantify the sensitivity of retrieval models. The model with the minimum theoretical error is chosen for experimental data analysis.

The theoretical error of a retrieval model can be derived by calculating the partial derivative of the formulas of the models. When one of characteristics of the selected model, such as X, is fixed, the theoretical errors of T and P on the other characteristic Y can be expressed as $\partial T/\partial Y \cdot \Delta Y$ and $\partial P/\partial Y \cdot \Delta Y$, respectively. Similarly, the theoretical errors of T and P on the characteristic X when Y is fixed are $\partial T/\partial X \cdot \Delta X$ and $\partial P/\partial X \cdot \Delta X$, respectively. ΔX and ΔY represent 1 MHz measurement errors.

The total theoretical error ΔT of temperature can be expressed as the sum of $\partial T/\partial X \cdot \Delta X$ and $\partial T/\partial Y \cdot \Delta Y$, and the total theoretical error ΔP of pressure can be expressed as the sum of $\partial P/\partial X \cdot \Delta X$ and $\partial P/\partial Y \cdot \Delta Y$. Therefore, the theoretical errors of one point on the model can be expressed as Equation (8) and Equation (9).

$$\Delta T = \frac{\partial T}{\partial X} \cdot \Delta x + \frac{\partial T}{\partial Y} \cdot \Delta y \tag{8}$$

$$\Delta P = \frac{\partial P}{\partial X} \cdot \Delta x + \frac{\partial P}{\partial Y} \cdot \Delta y \tag{9}$$

In practical applications, the theoretical errors of characteristics corresponding to one point on the model are not always 1 MHz. Generally, four kinds of cases, i.e., (1 MHz, 1 MHz), (−1 MHz, 1 MHz), (1 MHz, −1 MHz), and (−1 MHz, −1 MHz), may occur in the theoretical analysis of model retrieval error; moreover, the probability of occurrence corresponding to each case is unclear until now. Therefore, the upper limitation of the total retrieval error can be used to determine the optimal model, which is of less dependence on the characteristic error. That is to say, Equation (8) and Equation (9) can be improved as follows:

$$\Delta T_{\max} = \left| \frac{1}{N} \sum_{i=1}^{N} \frac{\partial T}{\partial X_i} \right| \cdot |\Delta x| + \left| \frac{1}{N} \sum_{i=1}^{N} \frac{\partial T}{\partial Y_i} \right| \cdot |\Delta y|, \tag{10}$$

$$\Delta P_{\max} = \left| \frac{1}{N} \sum_{i=1}^{N} \frac{\partial P}{\partial X_i} \right| \cdot |\Delta x| + \left| \frac{1}{N} \sum_{i=1}^{N} \frac{\partial P}{\partial Y_i} \right| \cdot |\Delta y|, \tag{11}$$

where N represents the number of points in the retrieval model, namely the 225 sets of error values. The upper limitations of the theoretical errors $\Delta T_{\max}$ and $\Delta P_{\max}$, which represent the mean values of retrieval errors corresponding to each point on the model, can be calculated by the aforementioned operation. For instance, the theoretical error of T on V_b and Γ_b can be expressed according to Equation (6) and Equation (7), as follows:

$$\begin{aligned} & \frac{\partial T}{\partial V_b} \cdot \Delta V_b \\ & = (-1767.28 + 1678.98V_b + 2010.6\Gamma_b - 467.445V_b^2 \\ & \quad - 761.4\Gamma_b^2 - 347.34V_b\Gamma_b) \cdot \Delta V_b \end{aligned} \tag{12}$$

$$\begin{aligned} & \frac{\partial T}{\partial \Gamma_b} \cdot \Delta \Gamma_b \\ & = (-1982.96 + 2072.42\Gamma_b + 2010.6V_b - 216.83\Gamma_b^2 \\ & \quad - 1522.8V_b\Gamma_b - 173.67V_b^2) \cdot \Delta \Gamma_b \end{aligned} \tag{13}$$

In the same way, the theoretical error of P on V_b and Γ_b can be expressed as follows:

$$\begin{aligned} \frac{\partial P}{\partial V_b} \cdot \Delta V_b =\ & (14.91 - 17.58V_b - 22.28/\Gamma_b + 2.56V_b \\ & - 2.31/\Gamma_b^2 - 23.30V_b/\Gamma_b) \cdot \Delta V_b \end{aligned} \tag{14}$$

$$\begin{aligned} \frac{\partial P}{\partial \Gamma_b} \cdot \Delta \Gamma_b =\ & (-8.56/\Gamma_b^2 - 1.36/\Gamma_b^3 + 22.28V_b/\Gamma_b^2 \\ & - 2.706/\Gamma_b^4 - 4.62V_b/\Gamma_b^3 - 11.65V_b^2/\Gamma_b^2) \cdot \Delta \Gamma_b \end{aligned} \tag{15}$$

Assigning the value 1 MHz to both ΔV_b and $\Delta \Gamma_b$, we can determine that the error of the temperature retrieval model based on Brillouin shift is 0.3059 K, and that the error of the temperature retrieval model based on Brillouin linewidth

TABLE 1. Brillouin shift (GHz) of N_2 by fitting the simulation spectrum of Tenti-S6 with V3 in different temperatures and pressures.

p (bar)	T (K)														
	210	220	230	240	250	260	270	280	290	300	310	320	330	340	350
0.1	0.630	0.642	0.653	0.664	0.675	0.686	0.696	0.705	0.715	0.726	0.738	0.755	0.765	0.775	0.793
0.2	0.742	0.752	0.761	0.770	0.779	0.787	0.795	0.803	0.811	0.818	0.826	0.833	0.840	0.848	0.855
0.3	0.801	0.812	0.823	0.834	0.844	0.855	0.865	0.875	0.885	0.895	0.905	0.914	0.924	0.933	0.943
0.4	0.842	0.854	0.865	0.876	0.887	0.898	0.909	0.919	0.930	0.941	0.951	0.961	0.972	0.982	0.992
0.5	0.873	0.884	0.898	0.909	0.920	0.932	0.943	0.954	0.964	0.975	0.986	0.996	1.007	1.017	1.027
0.6	0.898	0.910	0.922	0.936	0.947	0.958	0.971	0.982	0.993	1.004	1.014	1.024	1.035	1.046	1.056
0.7	0.919	0.931	0.945	0.957	0.969	0.982	0.994	1.005	1.016	1.029	1.039	1.050	1.060	1.070	1.081
0.8	0.937	0.949	0.964	0.976	0.988	1.002	1.013	1.024	1.037	1.049	1.060	1.071	1.082	1.093	1.103
0.9	0.951	0.966	0.978	0.993	1.005	1.018	1.031	1.042	1.054	1.067	1.078	1.089	1.100	1.112	1.122
1.0	0.963	0.978	0.992	1.006	1.020	1.032	1.045	1.058	1.070	1.081	1.094	1.106	1.116	1.128	1.140
1.1	0.974	0.989	1.004	1.018	1.032	1.046	1.059	1.071	1.084	1.096	1.107	1.119	1.132	1.143	1.154
1.2	0.984	0.999	1.014	1.029	1.043	1.057	1.070	1.083	1.096	1.108	1.121	1.133	1.144	1.155	1.168
1.3	0.992	1.008	1.023	1.038	1.052	1.066	1.080	1.094	1.107	1.120	1.133	1.144	1.156	1.169	1.180
1.4	0.998	1.015	1.031	1.046	1.061	1.075	1.089	1.103	1.116	1.129	1.142	1.155	1.167	1.180	1.190
1.5	1.004	1.022	1.038	1.054	1.069	1.084	1.098	1.112	1.125	1.138	1.151	1.164	1.177	1.189	1.201

is 0.1875 K. Meanwhile, the error for the pressure retrieval based on Brillouin shift is 0.0033 bar, and the error for the pressure retrieval based on Brillouin linewidth is −0.0013 bar. Using Equation (10) and Equation (11), we can calculate the maximal theoretical temperature and pressure retrieval error to be $\Delta T_{max} = 0.4934$ K and $\Delta P_{max} = 0.0045$ bar, respectively. Similarly, the errors of the other five groups of retrieval models can be calculated using the same method.

Besides the theoretical retrieval error, the uncertainty can be used to describe the dispersion of retrieval error. From Equations (10) and (11), we can obtain the error function as follows:

$$\Delta T = Q\left(T_X, T_Y\right), \tag{16}$$

$$\Delta P = U\left(P_X, P_Y\right), \tag{17}$$

where $|\partial T/\partial X| \cdot |\Delta X|$ is denoted as T_X, and $|\partial T/\partial Y| \cdot |\Delta Y|$ is denoted as T_Y. P_X and P_Y are treated in the same way.

The partial derivatives, $\partial Q/\partial T_X$, $\partial Q/\partial T_Y$, $\partial U/\partial T_X$, and $\partial U/\partial T_Y$, can be calculated from the error functions Q and U, respectively. The uncertainties of temperature retrieval error and pressure retrieval error can be written as Equation (18) and Equation (19), respectively.

$$\sigma_{\Delta T} = \left[\left(\frac{\partial Q}{\partial T_X}\right)^2 \sigma_{T_X}^2 + \left(\frac{\partial Q}{\partial T_Y}\right)^2 \sigma_{T_Y}^2 + 2\left(\frac{\partial Q}{\partial T_X}\right)\left(\frac{\partial Q}{\partial T_Y}\right)\sigma_{T_X T_Y}\right]^{1/2} \tag{18}$$

$$\sigma_{\Delta P} = \left[\left(\frac{\partial U}{\partial P_X}\right)^2 \sigma_{P_X}^2 + \left(\frac{\partial U}{\partial P_Y}\right)^2 \sigma_{P_Y}^2 + 2\left(\frac{\partial U}{\partial P_X}\right)\left(\frac{\partial U}{\partial P_Y}\right)\sigma_{P_X P_Y}\right]^{1/2} \tag{19}$$

In these two formulas, $\sigma_{T_X T_Y}$ represent the covariance of $|\partial T/\partial X| \cdot |\Delta X|$ and $|\partial T/\partial Y| \cdot |\Delta Y|$. $\sigma_{P_X P_Y}$ is the covariance of $|\partial P/\partial X| \cdot |\Delta X|$ and $|\partial P/\partial Y| \cdot |\Delta Y|$, σ_{T_X} and σ_{T_Y} are the standard deviations of $|\partial T/\partial X| \cdot |\Delta X|$ and $|\partial T/\partial Y| \cdot |\Delta Y|$, respectively, and σ_{P_X} and σ_{P_Y} are the standard deviations of $|\partial P/\partial X| \cdot |\Delta X|$ and $|\partial P/\partial Y| \cdot |\Delta Y|$, respectively.

Equations (18) and (19) are too complicated for the partial derivatives, such as $\partial Q/\partial T_X$ and $\partial Q/\partial T_Y$, to be obtained conveniently. Therefore, a similar expression, converted from Equations (18) and (19), for calculating the uncertainty of retrieval error in a time-saving way can be written as follows:

$$\sigma_{\Delta T} = \left[\sigma_{T_X}^2 + \sigma_{T_Y}^2 + 2\sigma_{T_X T_Y}\right]^{1/2}, \tag{20}$$

$$\sigma_{\Delta P} = \left[\sigma_{P_X}^2 + \sigma_{P_Y}^2 + 2\sigma_{P_X P_Y}\right]^{1/2}. \tag{21}$$

It is known to us that the similar expression can reduce the complexity in calculating the uncertainty of retrieval error on the premise of ensuring accuracy, especially for a retrieval model that consists of more characteristics. Theoretically, the upper limit of the retrieval error and the distribution property can be used to evaluate the possible occurrence of maximal retrieval error. It can be verified that its small value generally represents the optimal model for parameter retrieval in other cases. The maximal theoretical errors and

TABLE 2. Temperature retrieval errors and pressure retrieval errors of the models for the six groups.

Model	Retrieval error							
	$\partial T/\partial X \cdot \Delta X$ (K)	$\partial T/\partial Y \cdot \Delta Y$ (K)	ΔT_{max} (K)	$\sigma_{\Delta T}$	$\partial P/\partial X \cdot \Delta X$ (K)	$\partial P/\partial Y \cdot \Delta Y$ (K)	ΔP_{max} (bar)	$\sigma_{\Delta P}$
A	0.3057	0.1875	0.4932	0.0660	0.0033	−0.0013	0.0045	0.0024
B	0.1769	0.1775	0.3544	0.0511	0.0041	−0.0012	0.0053	0.0025
C	−0.7910	0.4864	1.2774	0.4525	0.0117	−0.0036	0.0153	0.0087
D	−0.1560	0.3314	0.4874	0.1079	0.0655	−0.1420	0.0062	0.0028
E	0.1254	0.1476	0.2731	0.0280	−0.0018	0.0014	0.0032	0.0014
F	**0.1388**	**0.0933**	**0.2321**	**0.0236**	**−0.0018**	**0.0020**	**0.0038**	**0.0011**

TABLE 3. Temperature retrieval errors and pressure retrieval errors of the three-parameter models for four groups.

Model	Retrieval error									
	$\partial T/\partial X\ \Delta X$ (K)	$\partial T/\partial Y \cdot \Delta Y$ (K)	$\partial T/\partial Z \cdot \Delta Z$ (K)	ΔT_{max} (K)	$\sigma_{\Delta T}$	$\partial P/\partial X \cdot \Delta X$ (bar)	$\partial P/\partial Y \cdot \Delta Y$ (bar)	$\partial P/\partial Z \cdot \Delta Z$ (bar)	ΔP_{max} (bar)	$\sigma_{\Delta P}$
G	0.1830	0.0697	0.1217	0.3745	0.0572	0.0036	−0.0008	−0.0005	0.0048	0.0026
H	−0.0910	0.1286	0.1306	0.3502	0.0537	0.0078	−0.0006	−0.0018	0.0102	0.0056
I	−0.0311	0.1191	0.1621	0.3124	0.0481	0.0055	−0.0009	−0.0010	0.0074	0.0040
J	**0.0924**	**0.0422**	**0.1278**	**0.2624**	**0.0404**	**−0.0013**	**-0.0005**	**0.0016**	**0.0034**	**0.0018**

their uncertainties calculated using Equations (10)–(11) and Equations (20)–(21), respectively, are all listed in Table 2.

It can be seen from Table 2 that the uncertainty of the temperature retrieval error based on Rayleigh linewidth Γ_R and whole RB scattering linewidth Γ_{RBS} (Group F) is minimum. The theoretical errors of temperature retrieval from Γ_R and Γ_{RBS} are 0.14 K and 0.09 K, respectively, and the maximal error is 0.23 K. In addition, the theoretical errors of pressure retrieval from Γ_R and Γ_{RBS} are −0.0018 bar and 0.0020 bar, respectively, and the total maximal error is 0.0038 bar. Although the maximal pressure retrieval error for Group E is less than that for Group F, the practical retrieval error would be larger than that for Group F, because the practical measured error of Brillouin linewidth would be larger than that of Rayleigh linewidth. In other words, for the dual-parameter model, the upper limit of retrieval error in a characteristic model is based on Rayleigh linewidth, and the overall spectral linewidth is minimal when the error of the characteristics is 1 MHz. The accuracy of the retrieval result is acceptable for real remote-sensing applications [16]–[19].

In the same way, the gas temperature and pressure can also be expressed as functions which consist of more characteristics (i.e., three-parameter or four-parameter retrieval model). The values of their maximal errors and the respective uncertainties are listed in Table 3 and Table 6. Furthermore, the fitting errors for the optimal group in each table, i.e., Group F, Group J, and Group K, are listed in Table 5.

Table 3 and Table 4 show that the three-parameter model based on Brillouin linewidth, Rayleigh linewidth, and RB spectral linewidth (Group J), and the four-parameter model based on Brillouin shift, Brillouin linewidth, Rayleigh linewidth, and RB spectral linewidth (Group K) are all optimum. In theory, the maximal temperature and pressure retrieval errors for Group J are 0.2624 K and 0.0034 bar, respectively. Meanwhile, the maximal temperature and pressure retrieval errors for Group K are 0.2989 K and 0.0062 bar. It is obvious that the errors of Group J and Group K are approximate to that of the dual-parameter retrieval model (Group F). From Table 5, we can see that the mean temperature and pressure fitting errors of Group F are minimal compared with those of the other groups, which indicate that Group F is of greater applicability for temperature and pressure retrieval.

TABLE 4. Temperature retrieval errors and pressure retrieval errors of the four-parameter models.

Model	Retrieval error											
	$\partial T/\partial X\cdot\Delta X$ (K)	$\partial T/\partial Y\cdot\Delta Y$ (K)	$\partial T/\partial Z\cdot\Delta Z$ (K)	$\partial T/\partial W\cdot\Delta W$ (K)	ΔT_{max} (K)	$\sigma_{\Delta T}$	$\partial P/\partial X\cdot\Delta X$ (bar)	$\partial P/\partial Y\cdot\Delta Y$ (bar)	$\partial P/\partial Z\cdot\Delta Z$ (bar)	$\partial P/\partial W\cdot\Delta W$ (bar)	ΔP_{max} (bar)	$\sigma_{\Delta P}$
K	**−0.0291**	**0.0863**	**0.0416**	**0.1419**	**0.2989**	**0.0460**	**0.0047**	**−0.0006**	**−0.0004**	**−0.0005**	**0.0062**	**0.0034**

TABLE 5. Fitting errors of the optimal retrieval models for three groups.

Model	Fitting error of temperature retrieval model				Fitting error of pressure retrieval model			
	Min (K)	Max (K)	Mean (K)	Std (K)	Min (bar)	Max (bar)	Mean (bar)	Std (bar)
F	**−5.3234**	**7.5516**	**0**	**1.7056**	**−0.1165**	**0.2492**	**0**	**0.0429**
J	**−5.9497**	**4.0557**	**−0.0139**	**1.8930**	**−0.1011**	**0.1099**	**−0.0039**	**0.0373**
K	**−5.5624**	**3.3709**	**−0.0136**	**1.7793**	**−0.0415**	**0.0896**	**0.0003**	**0.0193**

Note: In Table II, (X, Y) represent a group of spectral characteristic parameters, i.e., A (Brillouin shift, Brillouin linewidth), B (Brillouin shift, Rayleigh linewidth), C (Brillouin shift, RBS linewidth), D (Brillouin linewidth, Rayleigh linewidth), E (Brillouin linewidth, RBS linewidth), and F (Rayleigh linewidth, RBS linewidth). In Table III, Z represents another characteristics parameter, and G (Brillouin shift, Brillouin linewidth, Rayleigh linewidth), H (Brillouin shift, Rayleigh linewidth, RBS linewidth), I (Brillouin shift, Brillouin linewidth, RBS linewidth), and J (Brillouin linewidth, Rayleigh linewidth, RBS linewidth) represent 3-parameter retrieval models. In Table IV, W represents a new characteristics parameter, and K (Brillouin shift, Brillouin linewidth, Rayleigh linewidth, RBS linewidth) represents a 4-parameter retrieval model. In Table V, Min (K) and Min (bar) represent the minimum fitting errors of three kinds of temperature and pressure retrieval models, respectively, Max (K) and Max (bar) represent the maximum fitting errors of the temperature and pressure retrieval models, respectively, Mean (K) and Mean (bar) represent the average fitting errors of the temperature and pressure retrieval models, respectively, and Std(K) and Std(bar) represent the standard deviations of the temperature and pressure retrieval models, respectively.

TABLE 6. Retrieval errors for each model based on the characteristics of Rayleigh–Brillouin spectrum in N_2.

297 K	1.0 bar		0.75 bar		0.5 bar		0.3 bar		0.1 bar	
Model	ΔT (K)	ΔP (bar)	ΔT (K)	ΔP (bar)	ΔT (K)	ΔP (bar)	ΔT (K)	ΔP (bar)	ΔT (K)	ΔP (bar)
A	20.71	−0.02	26.79	0.03	36.88	0.36	−8.39	0.40	−80.46	0.03
B	7.08	0.10	7.25	0.17	16.19	0.52	12.59	0.32	−9.57	−0.05
C	−33.56	0.55	-53.04	0.78	−144.58	2.71	−101.55	1.37	3.00	−0.49
D	−7.25	−0.23	-3.31	−0.18	3.98	0.11	24.59	0.72	33.41	0.60
E	7.04	−0.16	5.08	−0.13	−9.17	0.01	−33.76	0.21	−32.77	0.21
F	**−0.24**	**−0.07**	**-0.34**	**−0.07**	**−1.87**	**−0.05**	**−0.75**	**−0.05**	**−1.56**	**0.02**
G	9.65	0.03	17.02	0.06	25.93	0.40	8.13	0.36	−39.63	0.01
H	−1.54	0.29	-6.74	0.42	−19.38	1.36	−19.63	0.71	6.85	−0.07
I	3.47	0.12	0.34	0.19	−16.94	0.77	−39.87	0.61	−30.98	−0.03
J	3.98	−0.16	2.40	−0.15	−9.72	−0.02	−28.54	0.14	−27.41	0.18
K	2.75	0.09	-0.06	0.14	−14.32	0.58	−31.45	0.45	−22.77	−0.02

The dual-parameter retrieval models based on Rayleigh linewidth Γ_R and whole RB scattering linewidth Γ_{RBS} (Group F) are expressed as Equation (22) and Equation (23):

$$\begin{aligned} T = {} & 114.08 + 253.15\Gamma_R - 341.51\Gamma_{RBS} \\ & - 104.34\Gamma_R^2 + 121.37\Gamma_{RBS}^2 \\ & + 42.68\Gamma_R\Gamma_{RBS} - 227.68\Gamma_R^3 \\ & + 145.92\Gamma_{RBS}^3 - 559.31\Gamma_R\Gamma_{RBS}^2 \\ & + 642.97\Gamma_R^2\Gamma_{RBS} \end{aligned} \tag{22}$$

$$\begin{aligned} P = {} & 7.36 - 17.26\Gamma_R + 6.41\Gamma_{RBS} + 11.63\Gamma_R^2 + 1.08\Gamma_{RBS}^2 \\ & - 7.46\Gamma_R\Gamma_{RBS} - 0.23\Gamma_R^3 \\ & - 1.01\Gamma_{RBS}^3 + 3.75\Gamma_R\Gamma_{RBS}^2 - 3.34\Gamma_R^2\Gamma_{RBS} \end{aligned} \tag{23}$$

Meanwhile, the three-parameter retrieval models (Group J) were expressed as Equation (24) and Equation (25):

$$T = \exp(0.33\Gamma_b + 0.15\Gamma_R + 0.46\Gamma_{RBS} + 3.67), \tag{24}$$

$$P = \exp(-1.67\Gamma_b - 0.64\Gamma_R + 1.94\Gamma_{RBS} - 2.49). \tag{25}$$

The four-parameter retrieval models (Group K), which is based on all characteristics of the RB spectrum, can be expressed as follows:

$$T = \exp(-0.1V_b + 0.31\Gamma_b + 0.15\Gamma_R + 0.51_{RBS} + 3.66) \tag{26}$$

$$P = \exp(5.38V_b - 0.795\Gamma_b - 0.55\Gamma_R - 0.597\Gamma_{RBS} - 2.457) \tag{27}$$

Retrieval models for air can be obtained the same way as for nitrogen. The equations of dual-parameter retrieval models in

air can be expressed as follows:

$$\begin{aligned} T =& -14.34 + 372.69\Gamma_R - 298.76\Gamma_{RBS} - 147.78\Gamma_R^2 \\ &+ 117.32\Gamma_{RBS}^2 + 22.42\Gamma_R\Gamma_{RBS} \\ &- 240.03\Gamma_R^3 + 158.04\Gamma_{RBS}^3 - 600.69\Gamma_R\Gamma_{RBS}^2 \\ &+ 694.68\Gamma_R^2\Gamma_{RBS} \end{aligned} \tag{28}$$

$$\begin{aligned} P =& 11.32 - 21.75\Gamma_R + 5.55\Gamma_{RBS} + 13.45\Gamma_R^2 \\ &+ 1.13\Gamma_{RBS}^2 - 6.91\Gamma_R\Gamma_{RBS} \\ &- 0.54\Gamma_R^3 - 0.96\Gamma_{RBS}^3 + 3.58\Gamma_R\Gamma_{RBS}^2 \\ &- 3.27\Gamma_R^2\Gamma_{RBS} \end{aligned} \tag{29}$$

The expressions for the three-parameter models can be written as follows:

$$T = \exp(0.34\Gamma_b + 0.15\Gamma_R + 0.47\Gamma_{RBS} + 3.67), \tag{30}$$

$$P = \exp(-1.76\Gamma_b - 0.61\Gamma_R + 1.96\Gamma_{RBS} - 2.49). \tag{31}$$

Certainly, the four-parameter models based on all characteristics can be expressed as

$$\begin{aligned} T =& \exp(2.518V_b + 0.344\Gamma_b + 0.148\Gamma_R \\ &+ 0.454\Gamma_{RBS} + 3.674) \end{aligned} \tag{32}$$

$$P = \exp(6.23V_b - 0.9\Gamma_b - 0.58\Gamma_R - 0.65\Gamma_{RBS} - 2.516) \tag{33}$$

The theoretical analysis shows that the three groups of models that depend on RB spectral characteristics are suitable for deriving the gas temperature and pressure simultaneously. Nevertheless, it can be seen in Table 2 that the maximal retrieval errors and uncertainties for Group F, which is based on Rayleigh linewidth and the whole spectral linewidth, have the minimum values. It can also be seen in Table 5 that the mean values of the fitting errors for Group F are at the minimum. Therefore, Group F is selected for the simultaneous retrieval of temperature and pressure, for whether the gas is nitrogen or air. However, the accuracies of temperature and pressure retrieval are not only influenced by the theoretical errors of the retrieval model but are also related to the measured errors for the RB spectral characteristics. A discussion on the measured errors of characteristics based on the practical RB scattering spectrum, for verifying the correctness of the theoretical analysis, is presented in the next section.

III. EXPERIMENTAL PROCEDURE AND RESULTS

A. EXPERIMENTAL CONDITION AND DATA PROCESSING

The RB scattering profiles were measured using a sensitive setup described in reference [5]. In this setup, a tunable laser (TI: SA) pumped by a MilleniaXs laser and at a power of 10 W produced a stable narrow-linewidth red light with a wavelength of 806 nm. This red light was directed into the doubling cavity and outputted blue light with a wavelength of 403 nm, which was then injected into the gas cell, and 90° scattered light was collected. Subsequently, the scattered light was projected into the Fabry–Pérot interferometer (FPI), and the RB spectrum was recorded by scanning the FPI through tuning its piezo voltage. Finally, the high-resolution RB scattering spectra were obtained from the photomultiplier tube (PMT) and then sent to a computer for experimental analysis. The RB spectra we used in the experiment are of a higher signal-to-noise ratio from averaging the several peaks (∼50) of the scattering RB spectra. Here, for the N_2 experiment, the instrumental linewidth (FWHM) of the FPI was 128 MHz, and the free spectral range (FSR), was 7.478 GHz, the frequency sweep span correspond to tens of effective FSRs [5]. For the air experiment, the instrumental linewidth (FWHM) of the FPI was 140 MHz, and the free spectral range (FSR) was 7.553 GHz. The frequency step of the RB spectrum we obtained was 40 MHz. The FPI we used in the experiment was homemade, and its parameters have been outlined in reference [5].

The temperature of the gas cell is controlled by a heating water cooling system and is measured by two Pt100 platinum resistances [5]. The maximal uncertainty of temperature measurement is less than 0.5 K. The pressure in the gas cell is measured by a pressure vacuum gauge, which was produced by Pfeiffer Vacuum, and its uncertainty is 0.5%. The material of the scattered cell is aluminum to ensure temperature stability for the experimental operation.

In the experiment, the light from the mirror of the gas cell and the inner wall of the cell will produce a narrow central peak for the RB scattering spectrum, which is regarded as the Mie scattering, as shown in Figure 2(a). Therefore, in this study, the function of V3+Mie is used to fit the RB scattering spectrum of the experimental data to reduce the effect of Mie scattering noise on fitting precision. The experimental RB scattering spectrum at a certain temperature and pressure is then expressed as follows:

$$F(T, p, v) = I_{RB} \cdot S_{RB}(T, p, v)^* Airy(v), \tag{34}$$

where I_{RB} is the intensity of the RB scattering spectrum, and S_{RB} is the RB scattering spectrum, which is represented as a V3+ Mie model. Here, the Mie function can be expressed as the convolution of Dirac delta function [30] and the instrumental function of FPI. Airy(v) is the instrumental function of an ideal FPI, the mirror of which does not have any defects, and can be expressed as Equation (35), according to [30].

$$Airy(v) = 1/\left(1 + \left(\frac{2FSR}{\pi FWHM}\right)^2 \sin^2\left(\frac{\pi v}{FSR}\right)\right) \tag{35}$$

In reality, the imperfection and irregularities on the surface of the FPI mirror cause a change in the intensity transmission and have remarkable influence on the accuracy of the RB spectrum line-shape analysis, which will lead to inaccuracies in the fitted parameters [31]. Additionally, the error between the parameter from fitting S6 with a Voigt function and that obtained from fitting experimental data with a Voigt + Mie function is the main factor that affects the accuracy of the retrieval model. Therefore, removing the instrumental function from the experimental RB spectra of nitrogen and air can reduce the influence of the instrument broadening on

the characteristic parameters that are derived. In the process of deconvolution, the experimental RB spectra are treated via fast Fourier transform (FFT) [31], [32]. According to Equation (34), the convolution of RB spectral line shape S_{RB} and the spectrum of the instrumental Airy function can be expressed as their individual Fourier transforms, as follows:

$$F_{RB}(k) = I_{RB} \cdot S'_{RB}(k) \cdot Airy'(k), \tag{36}$$

where the signals in the frequency regime have been converted into their related formation in k space ($\mathrm{k} = 2\pi\nu$). In this way, Fourier transformations of the RB spectrum and instrumental function are performed, and $S_{\mathrm{RB}}(\nu)$ can be derived via an inverse Fourier transform of $S'_{\mathrm{RB}}(\mathrm{k})$. Afterward, band-stop filter is used to decrease the noise from the deconvolution in FFT. Finally, the spectrum was compared with the Voigt + Mie function to obtain the inner component of the RB spectrum.

The process of deconvolution and the characteristics derived from the experimental spectrum can be visualized as in Figure 2.

B. ANALYSIS OF CHARACTERISTICS AND SELECTION OF SUITABLE RETRIEVAL MODEL

To the best of our knowledge, the measured error depends on many factors; for instance, the properties of each characteristic and the quality of the RB spectrum are affected by the signal-to-noise ratio (SNR) in different temperatures and pressures. The gas RB spectrum, as shown in Figure 1, indicates that the proportion of the Brillouin spectrum is less than that of the Rayleigh spectrum, and therefore, the noise interference would result in the measurement error of the Brillouin linewidth.

Another reason is related to the SNR of the Brillouin spectrum, which is decreased with the gas pressure falling. Based on this observation, the measurement of Brillouin linewidth will be inaccurate. In terms of the errors of additional characteristics, such as Brillouin linewidth or Brillouin shift, which were introduced into the retrieval result, the retrieval errors of the three-parameter model (Group J) and four-parameter model (Group K) will be larger than that of the dual-parameter model (Group F), even though the theoretical errors of the three- and four-parameter models are similar to that of the dual-parameter model.

Although the deconvolution could eliminate the influence of FPI on the deviation between measured and theoretical characteristics, the measured errors for Brillouin shift and Brillouin linewidth will increase with the decrease in gas pressure. Therefore, it is necessary to consider the measured error from the experimental RB spectrum when we select the suitable model for gas temperature and pressure retrieval. The N_2 experiment is performed to prove the validity of the retrieval model that was selected, and the deviations between measured and theoretical characteristics from the deconvoluted RB spectrum in the condition of different pressures are visualized in Figure 3.

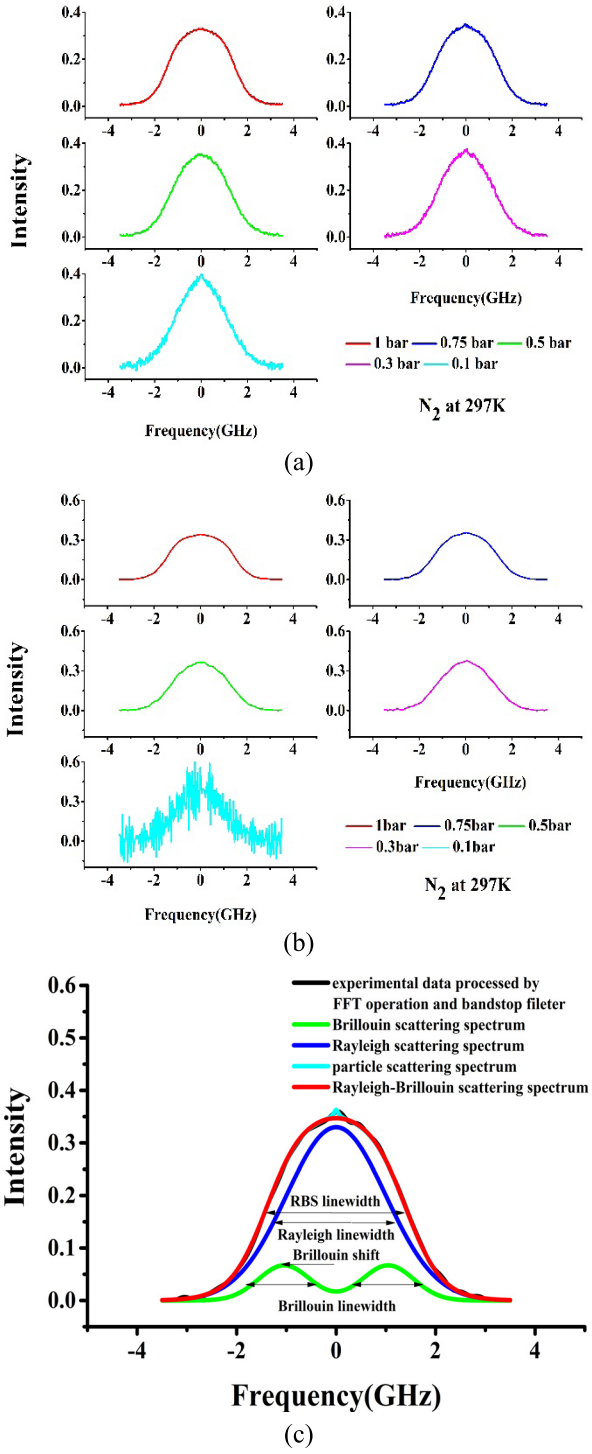

FIGURE 2. (a) Original experimental RB spectra of N_2, (b) deconvoluted experimental RB spectra of N_2, (c) spectra at 0.75 bar and 297 K as an example to show the characteristics derived from comparing the spectra with the 3V+Mie function.

Figure 3 shows that the Brillouin shift and Brillouin linewidth are of a larger measured error, especially in low pressures. Therefore, the models that contain Brillouin shift or Brillouin linewidth (e.g., Group E, J, K) are not suitable for the simultaneous retrieval of gas temperature

TABLE 7. Results of retrieval in air using the dual-parameter model based on Rayleigh linewidth and RBS linewidth.

	T_{Pt100} (K)	p (bar)	Γ_R (GHz)	Γ_{RBS} (GHz)	T_{model} (K)	P_{model} (bar)	Error (K)	Error (bar)	$\triangle T_{S6}$ (K)
Air ~1.0 bar	256.6	0.88	2.101	2.695	255.398	0.963	1.202	−0.083	1.628
	278.3	0.953	2.197	2.799	278.215	1.014	0.085	−0.061	−0.812
	295.8	1.012	2.269	2.888	296.875	1.086	−1.075	−0.074	1.614
	320.1	1.095	2.363	2.993	321.026	1.158	−0.926	−0.063	0.921
	339.9	1.165	2.435	3.076	340.355	1.219	−0.455	−0.054	0.390

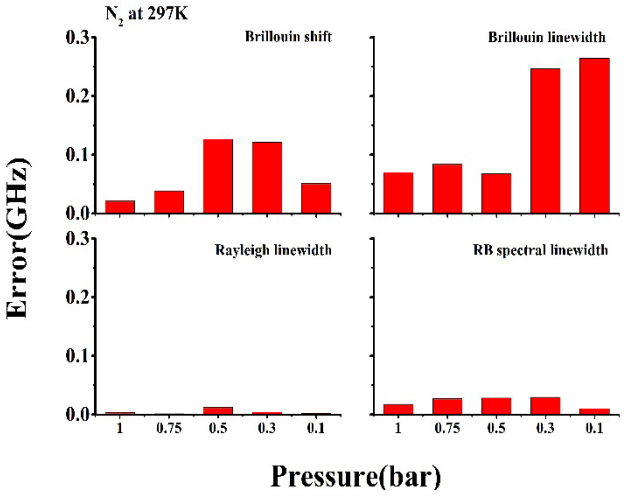

FIGURE 3. Characteristic deviations between the measurements and theoretical values for N_2 RB spectrum in 297 K and pressures from 1 bar to 0.1 bar.

and pressure. From a comparison of retrieval models using different numbers of characteristics, two characteristics are determined to be enough to accurately retrieve the gas temperature and pressure, because a larger retrieval error will be introduced from the measured errors of additional characteristics. Therefore, the precision of the dual-parameter retrieval model that depends on the Rayleigh linewidth and RB spectral linewidth indicates that the model is feasible for practical use.

C. RESULTS AND ANALYSIS

The RB scattering spectra of N_2 were measured at room temperature and at pressures of 0.1 bar, 0.3 bar, 0.5 bar, 0.75 bar, and 1.0 bar, corresponding to the pressure values of atmospheric environment at different altitudes, longitudes, and latitudes. Each characteristic of the RB scattering spectrum is obtained by fitting the deconvoluted RB scattering spectrum with the V3+ Mie model. The retrieval value of gas temperature and pressure can then be derived according to the retrieval models from Group A to Group K. The retrieval errors of each model are all listed in Table 6.

From the retrieval errors in Table 6, we can see that Group F is optimal, no matter what retrieval model we selected. This conclusion coincides with the theoretical error analysis for each retrieval model. The explicit reason may have resulted from the lower theoretical error for Group F; the dual-parameter model could avoid the additional retrieval error caused by the measured errors of additional characteristics in three- or four-parameter models. However, the retrieval errors for Group H and J may sometimes be less than that for Group F, when the measured errors of Brillouin shift and Brillouin linewidth can be decreased. For instance, the measurement of spectral Brillouin shift and Brillouin linewidth could become accurate by means of frequency correction and double-edge molecular technology. Therefore, the three-parameter models (Groups H and J) are also of significance in future research. Nevertheless, because of length limits, Group H and J are not the focus points of this study.

From the results in Table 6, we can see that the maximum retrieval errors of the model based on Rayleigh linewidth and the whole RB scattering linewidth at 0.3–1 bar meet the requirement for gas detection. The error for temperature retrieval at 0.1 bar, especially, reaches up to 1.56 K, which may have resulted from the RB spectral line shape simulated by the S6 model approximating a Gaussian line shape in a low-pressure situation [24], [33], [34], and the retrieval error would increase by means of the dual-parameter model. However, this error is smaller than the retrieval result derived from the whole linewidth of the spectrum [17], wherein the error of temperature retrieval is 2.9 K in N_2, and thus the dual-parameter retrieval method decreases the retrieval error by a large degree.

The performance of the dual-parameter model for real atmospheric remote sensing is further researched, and the retrieval results for air from the dual-parameter model in different temperature and pressure conditions are listed in Table 7. The pressure values adopted in the air experiment are close to 1.0 bar, with the temperatures ranging from 256 K to 340 K, which correspond to real atmospheric situations. The retrieval errors from the method presented in reference [15], [16] are all listed in Table 7 to interpret the optimal model we proposed for the simultaneous retrieval of gas temperature and pressure.

From the experimental data in Table 7, we can see that the maximum error for temperature retrieval in the retrieval model based on Rayleigh linewidth and the whole linewidth of RB spectral is 1.202 K, and the maximum error for pressure

retrieval is 0.083 bar. The temperature retrieval errors of the S6 line shape are also listed in Table 7. Compared with the temperature retrieval model based on the S6 line shape, the new method we proposed not only increases the temperature retrieval accuracy but also can realize air temperature and pressure retrieval simultaneously. Generally speaking, this dual-parameter retrieval model under construction is feasible for practical use.

IV. CONCLUSION

This paper is divided into two parts: theoretical simulation and experimental verification. In the simulation part, the characteristics of the RB scattering spectra of nitrogen and air in temperatures ranging from 210 to 350 K and pressures ranging from 0.1 to 1.5 bar were obtained by fitting the Tenti-S6 model with the V3 model. Based on the theoretical error analysis, the retrieval model with respect to Rayleigh linewidth and the whole RB scattering linewidth is determined to be optimal. In the experimental section, when the characteristics of the experimental RB scattering of nitrogen and air are obtained, the Mie scattering noise is considered, and the deconvolution is used to reduce the effect of the instrumental function on the accuracy of the fitted parameters. The errors between the retrieval results from the S6 model and the experimental spectrum are analyzed. For N_2, the errors for temperature and pressure retrieval can satisfy the requirement for real gas detection, especially in the case of pressure at 0.1 bar, when the error for temperature retrieval reaches only up to 1.56 K, which is lower than the result derived from other methods in low pressure. For air, the maximum error for temperature retrieval is 1.202 K, and the maximum error for pressure retrieval is 0.083 bar. The results show that utilizing the dual-parameter retrieval model to detect the temperature and pressure of gas in laboratory exhibits promise. As for the difference between laboratory conditions and the outdoor environment, further research would be performed on the application of lidar in real atmosphere. Nonetheless, the theoretical method proposed in this article is helpful and greatly promotes the development of Brillouin lidar remote sensing in future.

ACKNOWLEDGMENT

The authors would like to thank Wim Ubachs for provision of experimental data and thank Dr. Yuanqing Wang for his helpful discussions.

REFERENCES

[1] X.-G. Pan, M. N. Shneider, and R. B. Miles, "Coherent Rayleigh-Brillouin scattering," *Phys. Rev. Lett.*, vol. 89, no. 18, Oct. 2002, Art. no. 183001.
[2] Y. Anisimov, N. Kosykh, I. Mashek, and S. Smirnov, "Spectra of Rayleigh-Brillouin scattering in supersonic gas flows measured with a wide aperture spectrometer," *J. Phys, Conf. Ser.*, vol. 397, Dec. 2012, Art. no. 012048.
[3] Q. H. Lao, P. E. Schoen, and B. Chu, "Rayleigh-Brillouin scattering of gases with internal relaxation," *J. Chem. Phys.*, vol. 64, no. 9, pp. 3547–3555, May 1976.
[4] R. B. Miles, W. R. Lempert, and J. N. Forkey, "Laser Rayleigh scattering," *Meas. Sci. Technol.*, vol. 12, no. 5, pp. 33–51, Feb. 2001.
[5] Z. Gu and W. Ubachs, "A systematic study of Rayleigh-Brillouin scattering in air, N_2, and O_2 gases," *J. Chem. Phys.*, vol. 141, no. 10, Sep. 2014, Art. no. 104320.
[6] A. Gerakis, M. N. Shneider, and B. C. Stratton, "Remote-sensing gas measurements with coherent Rayleigh-Brillouin scattering," *Appl. Phys. Lett.*, vol. 109, no. 3, Jul. 2016, Art. no. 031112.
[7] M. Guo, J. Li, C. Sheng, J. Xu, and L. Wu, "A review of wetland remote sensing," *Sensors*, vol. 17, no. 4, pp. 777–812, Apr. 2017.
[8] J. W. Hair, C. A. Hostetler, A. L. Cook, D. B. Harper, R. A. Ferrare, T. L. Mack, W. Welch, L. R. Izquierdo, and F. E. Hovis, "Airborne high spectral resolution lidar for profiling aerosol optical properties," *Appl. Opt.*, vol. 47, no. 36, p. 6734, Dec. 2008.
[9] E. Hammann, A. Behrendt, F. Le Mounier, and V. Wulfmeyer, "Temperature profiling of the atmospheric boundary layer with rotational Raman lidar during the HD(CP)^2 observational prototype experiment," *Atmos. Chem. Phys.*, vol. 15, no. 5, pp. 2867–2881, Mar. 2015.
[10] Z.-B. Wang, P.-L. Yang, B.-B. Shao, M.-M. Tao, Y. Wu, and J.-J. Wu, "Fiber Bragg grating dual-parameter sensors for simultaneous stress and temperature measurements," *Laser Optoelectron. Prog.*, vol. 50, no. 10, pp. 56–60, Aug. 2013.
[11] K. Liang, "Research on simultaneous measurement of ocean temperature and salinity using Brillouin shift and linewidth," *Opt. Eng.*, vol. 51, no. 6, Jun. 2012, Art. no. 066002.
[12] C. D. Boley, R. C. Desai, and G. Tenti, "Kinetic models and Brillouin scattering in a molecular gas," *Can. J. Phys.*, vol. 50, no. 18, pp. 2158–2173, Sep. 1972.
[13] C. S. W. Chang, G. E. Uhlenbeck, and J. De Boer, "The heat conductivity and viscosity of poly-atomic gases," *Stud. Stat. Mech.*, pp. 241–268, 1964.
[14] X. Pan, M. Shneider, Z. Zhang, and R. Miles, "Bulk viscosity measurements using coherent Rayleigh-Brillouin scattering," in *Proc. 42nd AIAA Aerosp. Sci. Meeting Exhib.*, Reno, NV, USA, Jan. 2004, pp. 1–7.
[15] B. Witschas, C. Lemmerz, and O. Reitebuch, "Daytime measurements of atmospheric temperature profiles (2-15 km) by lidar utilizing Rayleigh-Brillouin scattering," *Opt. Lett.*, vol. 39, no. 7, p. 1972, Apr. 2014.
[16] B. Witschas, O. Reitebuch, C. Lemmerz, P. G. Kableka, S. Kondratyev, Z. Gu, and W. Ubachs, "The measurement of tropospheric temperature profiles using Rayleigh-Brillouin scattering: Results from laboratory and atmospheric studies," *EPJ Web Conf.*, vol. 119, 2016, Art. no. 27004.
[17] K. Liang, J. Xu, P. Zhang, Y. Wang, Q. Niu, L. Peng, and B. Zhou, "Temperature dependence of the Rayleigh Brillouin spectrum linewidth in air and nitrogen," *Sensors*, vol. 17, no. 7, p. 1503, Jun. 2017.
[18] M. Alpers, R. Eixmann, C. Fricke-Begemann, M. Gerding, and J. Höffner, "Temperature lidar measurements from 1 to 105 km altitude using resonance, Rayleigh, and rotational Raman scattering," *Atmos. Chem. Phys. Discuss.*, vol. 4, no. 1, pp. 923–938, Apr. 2010.
[19] P. Mateus, G. Nico, and J. Catalao, "Maps of PWV temporal changes by SAR interferometry: A study on the properties of atmosphere's temperature profiles," *IEEE Geosci. Remote Sens. Lett.*, vol. 11, no. 12, pp. 2065–2069, Dec. 2014.
[20] D. P. Vázquez, F. J. O. Reyes, and L. A. Arboledas, "A comparative study of algorithms for estimating land surface temperature from AVHRR Data," *Remote Sens. Environ.*, vol. 62, no. 3, pp. 215–222, Dec. 1997.
[21] *Atmosphere U.S. Standard, National Oceanic and Atmospheric Administration. National Aeronautics and Space Administration*, United States Air Force, Washington, DC, USA, 1976.
[22] H. Stocker, *Physics Handbook*. Beijing, China: Peking Univ. Press, 2004.
[23] B. Witschas, "Analytical model for Rayleigh-Brillouin line shapes in air: Errata," *Appl. Opt.*, vol. 50, no. 29, p. 5758, Oct. 2011.
[24] Y. Ma, F. Fan, K. Liang, H. Li, Y. Yu, and B. Zhou, "An analytical model for Rayleigh-Brillouin scattering spectrum in gases," *J. Opt.*, vol. 14, no. 9, Sep. 2012, Art. no. 095703.
[25] Y. Ma, H. Li, Z. Gu, W. Ubachs, Y. Yu, J. Huang, B. Zhou, Y. Wang, and K. Liang, "Analysis of Rayleigh-Brillouin spectral profiles and Brillouin shifts in nitrogen gas and air," *Opt. Express*, vol. 22, no. 2, p. 2092, Jan. 2014.
[26] J. A. Lock, R. G. Seasholtz, and W. T. John, "Rayleigh-Brillouin scattering to determine one-dimensional temperature and number density profiles of a gas flow field," *Appl. Opt.*, vol. 31, no. 15, p. 2839, May 1992.
[27] S.-I. Sato, "Theory for quantum interference signal from an inhomogeneously broadened two-level system excited by an optically phase-controlled laser-pulse pair," *J. Chem. Theory Comput.*, vol. 3, no. 3, pp. 1158–1162, May 2007.
[28] E. Whiting, "An empirical approximation to the Voigt profile," *J. Quant. Spectrosc. Radiat. Transf.*, vol. 8, no. 6, pp. 1379–1384, Jun. 1968.

[29] Z. Wan and Z.-L. Li, "A physics-based algorithm for retrieving land-surface emissivity and temperature from EOS/MODIS data," *IEEE Trans. Geosci. Remote Sens.*, vol. 35, no. 4, pp. 980–996, Jul. 1997.
[30] B. Witschas, Z. Gu, and W. Ubachs, "Temperature retrieval from Rayleigh-Brillouin scattering profiles measured in air," *Opt. Express*, vol. 22, no. 24, Dec. 2014, Art. no. 29655.
[31] B. Witschas, C. Lemmerz, and O. Reitebuch, "Horizontal lidar measurements for the proof of spontaneous Rayleigh-Brillouin scattering in the atmosphere," *Appl. Opt.*, vol. 51, no. 25, p. 6207, Sep. 2012.
[32] W.-H. Guo, Y.-Z. Huang, C.-L. Han, and L.-J. Yu, "Measurement of gain spectrum for Fabry–Pérot semiconductor lasers by the Fourier transform method with a deconvolution process," *IEEE J. Quantum Electron.*, vol. 39, no. 6, pp. 716–721, Jun. 2003.
[33] X. Pan, P. F. Barker, A. Meschanov, J. H. Grinstead, M. N. Shneider, and R. B. Miles, "Temperature measurements by coherent Rayleigh scattering," *Opt. Lett.*, vol. 27, no. 3, p. 161, Feb. 2002.
[34] L. Wu, J. M. Reese, and Y.-H. Zhang, "Temperature retrieval error in Rayleigh-Brillouin scattering using Tenti's S6 kinetic model," *AIP Conf. Proc.*, vol. 1786, no. 1, Nov. 2016, Art. no. 040010.

PENG ZHANG received the B.S. degree from Henan Agricultural University, Zhengzhou, China, in 2012, and the M.S. degree in electronic and communication engineering from Shaanxi Normal University, Xi'an, China, in 2015. He is currently pursuing the Ph.D. degree with the Department of Electronics and Information Engineering, Huazhong University of Science and Technology, Wuhan, China. His general field of research is signal and systems. His research interests include lidar remote sensing and detection, particularly in the area of the Rayleigh–Brillouin lidar remote sensing in atmosphere.

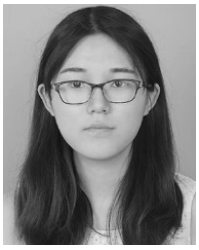

JIAQI XU was born in Wuhan, China, in 1995. She received the B.S. degree in communication engineering from the Wuhan University of Technology and the M.E. degree in electronic circuit and systems from the Huazhong University of Science and Technology, where she is currently pursuing the Ph.D. degree in electronic circuit and systems. Her general fields of research are in signal and systems. Her current research interest includes the remote sensing of the lidar and information processing.

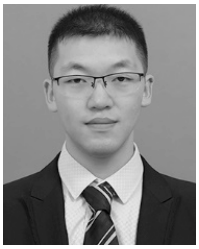

RUIZHE ZHANG received the B.S. degree in electronic science and technology from the Huazhong University of Science and Technology, Wuhan, China, in 2018, where he is currently pursuing the M.S. degree in circuits and systems.

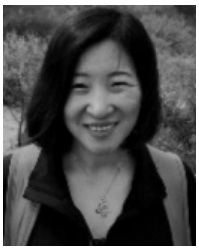

QIAN SUN received the degree from the Key Laboratory of Condensed Matter, Beihang University (BUAA), and the Ph.D. degree in physics from the Department of Physics, BUAA, in 2012. From 2012 to 2016, she was an Engineer with the Beijing Institute of Space Mechanics and Electricity. She is currently a Senior Engineer with the Beijing Institute of Space Mechanics and Electricity. Her current research interests include metamaterials, spectropy imaging, and remote sensing.

HANG WU received the B.S. degree in measurement and control technology and instruments from the China University of Geosciences, Wuhan, China, in 2018. He is currently pursuing the M.S. degree with the China Ship Development and Design Center, China Ship Research and Development Academy, Wuhan. From 2017 to 2018, his general field of research is image processing. His research interest includes the remote sensing of temperature-based Rayleigh Brillouin lidar, particularly in the area of the Rayleigh–Brillouin lidar remote sensing in sea.

YANGRUI XU is currently pursuing the M.S. degree in mechanical engineering with the Huazhong University of Science and Technology, Wuhan, China. His research interests include the deep learning, and the design and analysis of algorithms in lidars.

BO ZHOU received the Ph.D. degree from the Huazhong University of Science and Technology, Wuhan, China, in 2010. He is an Associate Professor with the School of Electronic Information and Communications, Huazhong University of Science and Technology. His general field of research is in circuits and systems. His current research interests include infrared image processing, circuits and systems, and remote sensing of the lidar.

KUN LIANG received the B.S., M.S., and the Ph.D. degrees in information and communication engineering from the Huazhong University of Science and Technology (HUST), Wuhan, China, in 2005 and 2008, respectively.

From 2008 to 2009, he was a Research Assistant with the Institute of Physics, Academia Sinica, Tapei, Taiwan. From 2014 to 2015, he was a Visiting Scholar with the Department of Physics and Astronomy, LaserLaB, VU University Amsterdam. He is currently an Associate Professor with the School of Electronic Information and Communications, (HUST). His general field of research is in signal and systems. His current research interests include infrared image processing, circuits and systems, remote sensing of the lidar, the development of surface processing and biological/medical treatment techniques using nonthermal atmospheric pressure plasmas, the fundamental study of plasma sources, and the fabrication of micro- or nano-structured surfaces.